

CIVA Computed Tomography Modeling

Roman FERNANDEZ¹, Marius COSTIN²,

David TISSEUR², Arnaud LEVEQUE², Samuel LEGOUPIL²

(1) EXTENDE, 86 rue de Paris, 91400, Orsay, France

(2) CEA, LIST, F-91191, Gif-sur-Yvette, France

Key-words: X-ray, modeling, tomography

Abstract

A new X-Ray computed tomography (CT) simulation module has recently been integrated into the CIVA software which completes the already available UT, ET and RT modules. The X-ray simulation software CIVA has been developed to help the design stage of radiographic systems, to enable performance demonstration and to optimize the testing process [1], [2]. In this context and to enlarge the capabilities of CIVA, the new computed tomography module is based on the RT module and takes benefit off all the tools already available in it.

In this paper, we present an overview of the functionalities available in the CIVA CT module, with a description of the different reconstruction algorithms already implemented in CIVA. This paper also illustrates a validation procedure of the X-ray RT module and proposes a typical application case.

1. Introduction

X-ray Computed Tomography imaging is recognized to be a complete and valuable non-destructive testing (NDT) method, taking advantage of the important progress of X-ray sources, detectors and of the reconstruction methods. Because of its high complexity, the modeling of a CT system is mandatory to optimize the system parameters for a given sample, and to evaluate its performances in terms of metrological accuracy and detection limits.

To meet this need, X-ray CT modeling software has been developed in the framework of the CIVA software. CIVA is a multi technique modeling software for NDT methods, such as ultrasonic inspection, Eddy current and X-ray methods, operating on Windows OS. The X-ray module (CIVA RT) models the full physics of photon-matter interaction in the range of 0.01 to 10MeV, including photons scattering. It allows the definition of the photon source parameters (gamma ray, X-ray spectrum or user defined spectra), the 3D object (IGES, CATIA or STL format) and material, the X-ray detection (radiographic film, CsI, CDD, pixels size, MTF...), the inclusion of calibrated defects in the object and the inspection geometry. The X-ray spot size, the forced Monte Carlo calculation parameters for photons scattering and the exposure time can also be defined. The accuracy of the computation has been compared to the MCNP4 and Penelope Monte Carlo software, showing that CIVA results are in a very good agreement even at high build-up factors.

Based on its X-ray module, CIVA software has recently been extended to tomography, with the same objective. In addition to X-ray inspection parameters, specific parameters to tomography, such as source to axis or source to detector distances and number of projections, can be selected. In the current version, two algorithms are implemented. To facilitate the comparison of more algorithms on a same set of data, the software implementation for the

reconstruction module is based on a plug-in process. A recent innovative method based on the Compressed Sensing approach has also been implemented following that procedure.

The CIVA Tomography modeling offers a unique platform to optimize CT system accurately, by simulating photons interactions, to compare algorithms in the same framework, to estimate the influence of SNR in projections or the number of projections. Effects of misalignments or object displacement during the acquisition process can also be estimated.

2. Principle

2.1 From radiography testing to computed tomography

In addition to X-Ray inspection parameters, the new CIVA 10.1 version includes specific tools linked to the tomography technique. All the options already available in the RT module are integrated in the CT module. In particular, the user can import a realistic complex 3D CAD component and can take into account the most influential parameters of a radiographic inspection.

In order to model a realistic inspection, either in the Radiography Testing simulation module or in the Computed Tomography module, CIVA combines an analytical model and a Monte-Carlo method.

The analytical model is used to calculate the images created from the direct radiation, while the Monte-Carlo model allows the simulation of the scattering effect. A combination of both models is then performed to give a realistic image [3] and [4].

Based on these computation methods, new positioning tools and tomography scanning are available in the computed tomography module.

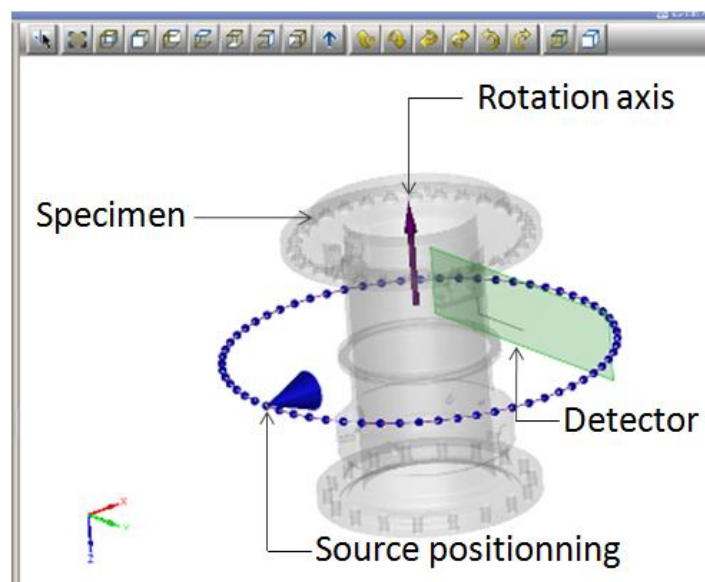


Figure 1. CIVA CT 3D view and tomography displacement in CIVA

The user will define different parameters such as the detector to rotation axis distance, the source to rotation axis distance, the orientation and the position of the rotation axis.

To produce a CT image, the source and the detector rotate around the specimen. CIVA computes all the RT simulations for all the defined projections and then simulates the radiographic inspection for all the source-detector positions.

2.2 Reconstruction Methods

Several CT reconstruction algorithms are implemented as plugins. This choice offers the possibility to implement various algorithms on different hardware, based on simple conventions for data input and output. Currently, two reconstruction algorithms are available in the commercial version of CIVA (FDK and PixTV) and several others are in development.

2.2.1 FDK

The FDK (Feldkamp-Davis-Kress) [5] algorithm is a 3D Fourier-based reconstruction method, as the gold standard in CT when SNR and projections number are large enough. We consider here the cone-beam geometry with a planar detector with equi-spaced pixels. The algorithm reconstructs the function $f(x,y,z)$, which is a map of the linear attenuation coefficients of the imaged sample, from the set of X-ray projections $p_{\beta}(r,\zeta)$ by using:

$$f(x, y, z) = \Delta\beta \sum_{i=1}^M \frac{1}{U_{\beta_i}^2} p_{\beta_i}^{wf}(r_{xy}, r_z)$$

where $p_{\beta_i}^{wf}(r_{xy}, r_z)$ are the weighted and ramp filtered projections, with r_{xy} and r_z the coordinates of the pixel that identifies the ray passing through the point (x,y,z) at the angular position β_i . This algorithm is implemented on CPU and parallelized for multi-core architectures.

2.2.2 PixTV

PixTV is an iterative reconstruction algorithm which minimizes the TV (total variation) norm. It uses the linear data model for the CT problem like the classical deterministic algorithms (e.g. ART). The projections and the imaged objects are discretized, i.e. they are represented by vectors or matrices. In the fan beam case (2D), a projection is written as:

$$p_k = \sum_{l=0}^N a_{k,l} \cdot f_l$$

where p_k is a vector containing the projection data for a ray k , $N = n^2$ is the total number of pixels, A is the system matrix containing the weights for all the pixels, and f is the vector containing the attenuation values which are to be recovered. The rays are considered as being completely independent, ranging from 0 to M , where $M = M_p \times N_{det}$ is the total number of projections in the fans at all angular positions, with M_p the number of angular projections and N_{det} the number of elements in the detector array.

PixTV is an optimized implementation [6] of the TVAL3 algorithm [7]. It models the CT problem in three ways. We present here only one, which is the most used:

$$\min_f \frac{\mu}{2} \|Af - p\|^2 + \|f\|_{TV}, s.t. f \in C$$

where μ is a penalty coefficient, A represents the system matrix and C a constraint set of possible solutions.

PixTV algorithm

Initialization : $f^0 = 0, k=0$ *while* not-converged *do* *while* iteration TV not-converged *do* compute projection $p^{k+1} \leftarrow \arg \min_y \mathcal{L}_{\mathcal{A}}(f^k, u, p; v, \lambda)$ compute auxiliary variable $u^{k+1} \leftarrow \arg \min_u \mathcal{L}_{\mathcal{A}}(f^k, u, p; v, \lambda)$ estimate solution $f^{k+1} \leftarrow \arg \min_f \mathcal{L}_{\mathcal{A}}(f, u^{k+1}, p^{k+1}; v, \lambda)$ *end while* $v \leftarrow v - \beta(Df^{k+1} - u^{k+1})$ $\lambda \leftarrow \lambda - \mu(Af^{k+1} - b - p^{k+1})$ $k \leftarrow k + 1$ *end while*

where $\mathcal{L}_{\mathcal{A}}(f, u, p; v, \lambda)$ is the augmented Lagrangian function.

2.2.3 BlobTV

The BlobTV algorithm is similar to the PixTV, but uses a different representation of the images [6]. Instead of using the pixel based representation, the images are discretized on a *blob* basis. The blobs are radial basis functions which may be used to decompose a continuous function. The main advantage of such a representation is the fact that most of the images can be decomposed with relatively few coefficients, and good quality reconstructions can be obtained from a small number of projections.

2.2.4 GradTV

The GradTV algorithm is a 3D iterative reconstruction using a simple gradient descent method to solve the CT problem, which is considered as a linear data model. Its particularity is the use of a TV regularization step on each iteration, which shows an important improvement of the results in cases of reconstructions from a small number of projections. The algorithm is implemented on GPU, and a special processing for large data sets is used.

GradTV algorithm

Initialization : $f^0 = 0, k=0$ *while* not-converged *do* compute projection $p^k \leftarrow FwdProj(f^k)$ update solution $f_{int}^{k+1} \leftarrow f^k + \lambda * BackProj(p - p^k)$ TV regularization $f^{k+1} \leftarrow RegTV(f_{int}^{k+1})$ $k \leftarrow k + 1$ *end while*

3. Applications

3.1 Scattering estimation validation

In order to validate the estimation of scattered photons, comparisons with the Penelope code have been conducted. Figure 5 presents the Civa and Penelope profiles obtained for mono-directional Cobalt-60 photons irradiating a stainless steel block perpendicularly to its surface. The thickness of the block is 100mm and the film is placed on the back face of the block. In

this configuration, the build-up ratio in photons number is estimated to be 4.6. The agreement is very good. Based on numerous equivalent simulations, we conclude that the scattering estimation of Civa is approved.

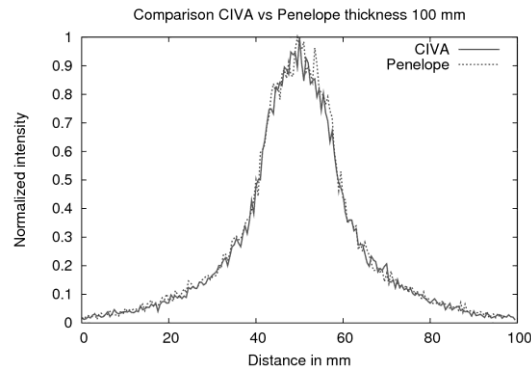


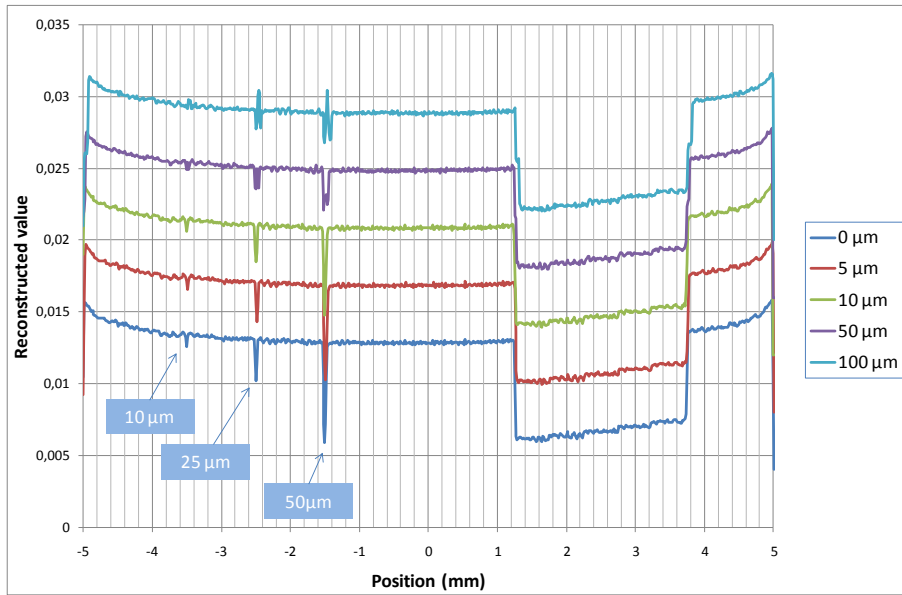
Figure 5. Comparison of the scattered intensity beam profile obtained with CIVA 10 (continuous line) and Penelope (dash line) for a thickness of 100 mm. Results show a perfect agreement between CIVA 10 and Penelope.

3.2 Example of Source/detector misalignment

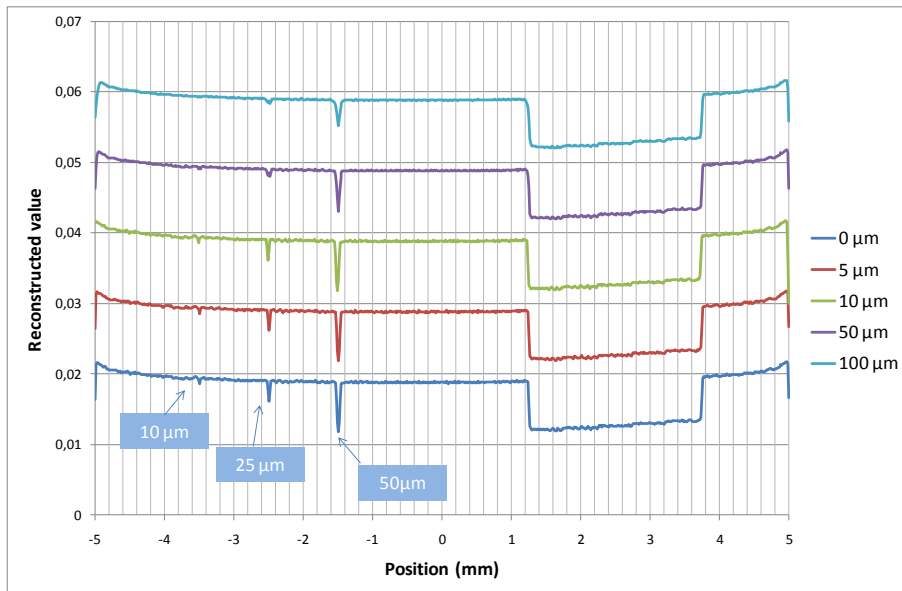
We propose to evaluate the influence of the X-ray spot size in a micro-CT configuration. We consider a CsI X-ray detector with a thickness of $300\mu\text{m}$ and a pixel binning of $50\mu\text{m}$. The value of MTF at 0.2% of the Hamamatsu C7942 detector has been estimated equal to $90\mu\text{m}$. The source to object distance and source to detector distance are set to 50mm and 200mm respectively for a magnification ratio of 4. The number of projections is 360 for all simulations. Images are reconstructed with FDK. The object is an Aluminum cylinder of 10mm in diameter. Two sets of aligned holes of diameter 5, 10, 25, $50\mu\text{m}$ and 50,100, 250 and $500\mu\text{m}$ have been inserted as well as 5 stacked carbon blocks sizing $500\times 1000\mu\text{m}$ with densities equal to 0.8, 1.0, 1.2, 1.4 and $1.6\text{g}/\text{cm}^3$. The X-ray tube operates at 90kV.

A first set of simulations has been conducted to estimate the influence of the rotation axis mispositioning. The rotation axis has been shifted perpendicularly in the horizontal plane with 5, 10, 50 and $100\mu\text{m}$. The Figure 6(a) presents the obtained results as profiles in the reconstructed 2D mid-plane image passing through the finest holes of the sample. The finest hole ($5\mu\text{m}$) cannot be detected, even with perfect alignment. Up to a misalignment of $10\mu\text{m}$, the second finest hole ($10\mu\text{m}$) is visible in the profile. The larger holes can be detected but their profile is distorted. Finally, the edges of carbon blocks are less sharp for large misalignment values.

A second set of simulations has been conducted where the X-ray spot size has been set to 0, 5, 10, 50 and $200\mu\text{m}$. The results are presented Figure 6(b), similarly to the previous results. As observed on the profiles plot, the $10\mu\text{m}$ hole cannot be detected when using a spot size larger than $10\mu\text{m}$.



(a)



(b)

Figure 6 Influence of rotation axis mispositioning (a) and X-ray source size (b) on reconstructed profile

3.3 Comparison study

A comparison study has been performed on a complex numerical object in order to evaluate the performance of the presented reconstruction algorithms. The scene as defined in CIVA is displayed in figure 2.

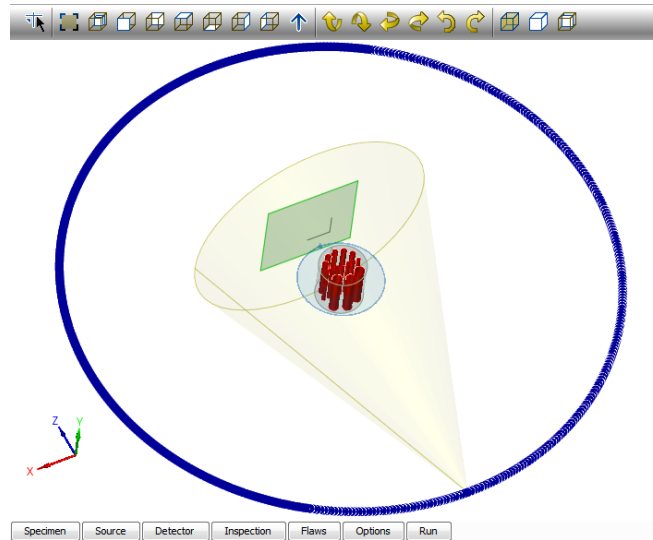


Figure 2. CIVA scene and CT setup for the comparison study.

The X-ray source is a reflection type X-ray generator, set to an acceleration voltage of 100kV and a target current of 10mA. The sample is a Plexiglas cylinder of 50mm in diameter, containing 15 cylindrical insertions of different materials and densities. The largest three cylinders are respectively tissue equivalent, bone and Aluminum, with their theoretical densities. In the opposite series of cylinders, the first (right to left order) is in air and the other four in water equivalent with a density ranging from 0.5g/cm^3 to 2.0g/cm^3 . The central series is also in water equivalent, with densities ranging from 0.7g/cm^3 to 1.3g/cm^3 in steps of 0.1g/cm^3 . The detector is a flat panel type with 512×512 pixels with a pitch of $200\mu\text{m}$.

A number of 512 projections equally distributed over a full rotation were simulated taking into account the photonic noise. In the projection images the SNR was estimated to approximately 50dB.

We first present a qualitative comparison by showing the reconstructions of the central plane from the complete set of projections.

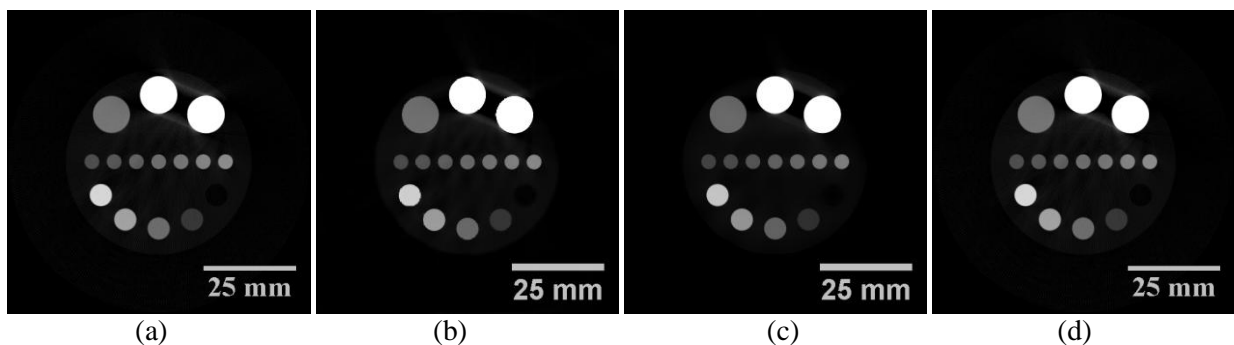


Figure 3. Qualitative comparison, reconstructions from the full data set:
 (a) FDK, (b) PixTV, (c) BlobTV and (d) GradTV

Qualitatively, the results are very similar to what is normally expected. The artefacts around the large cylinders are produced by their high attenuation, and it appears that the regularisation used in PixTV and BlobTV is more effective in reducing this type of artefacts.

A more interesting study is the evaluation for the cases of reconstruction from a lower number of projections. Figure 4 presents the reconstructions from 32 equi-distributed projections, extracted from the full data set.

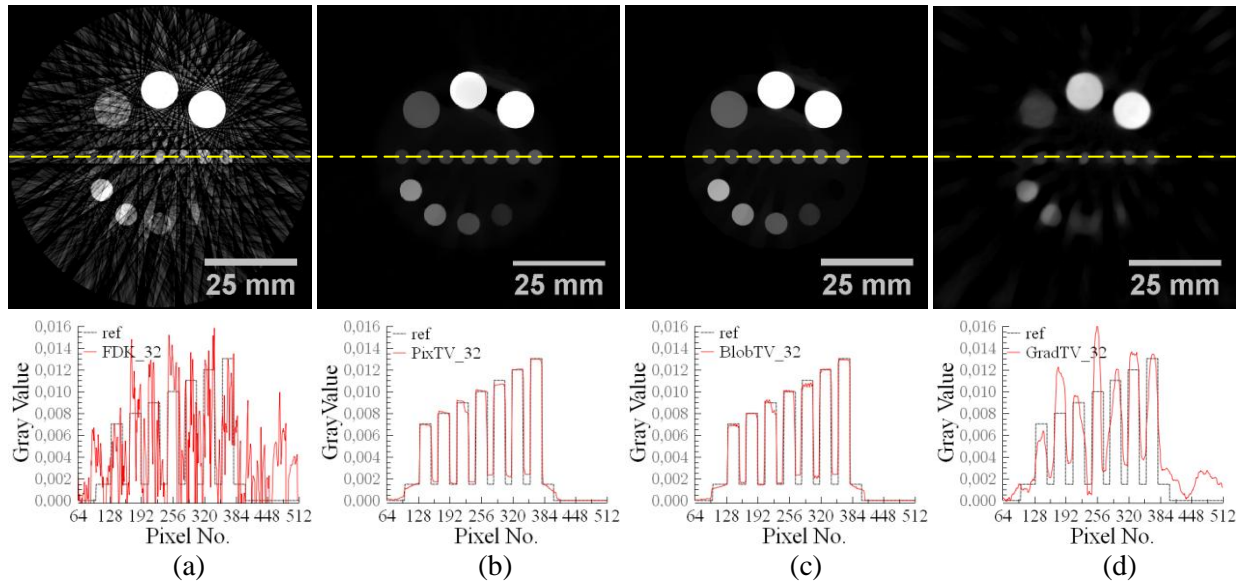


Figure 4. Reconstructions from 32 projections and profile plots along the central series of cylinders: (a) FDK, (b) PixTV, (c) BlobTV and (d) GradTV

The advantages for this case are clearly in favour of the iterative algorithms (b), (c) and (d) as compared to the FDK reconstruction (a), which is strongly affected by streak artefacts. The PixTV and BlobTV images are very similar and give the most accurate results. The GradTV image is better than the FDK, but much of the information is lost, the contours of the cylinders are deformed and the gray values contain large errors.

4. Conclusion

Nowadays, computed tomography is a powerful nondestructive evaluation (NDE) technique capable to provide information on the internal structure and geometry of an object.

Based on the RT module, the CIVA CT module meets the specific requirements of computed tomography modeling for many applications, by benefiting from all the contributions of the RT module.

This paper illustrates two algorithms used for reconstruction already available in the commercial release of CIVA and two other algorithms in the validation phase.

This new module allows the users to optimize the acquisition methods and to prepare inspections, by using the ability to carry out exhaustive parametric studies, to assess influential parameters, and also, alongside an inspection, to determine if deviations from inspection procedures are critical. Finally, this paper illustrates a typical problem that can be

encountered during CT acquisition, which is the evaluation of the influence of X-ray spot size in a micro-CT configuration and a source/detector misalignment.

Experimental validations of the X-Ray CT module have already been performed with a SkyScan 2011 nano-tomograph and other validations and acquisition/simulations comparisons are in progress.

5. References

- [1] R. Fernandez, A. Schumm, J. Tabary, P. Hugonnard, «Simulation studies of radiographic inspections with CIVA», 17th WCNDT, 2008.
- [2] A. Schumm, R. Fernandez, J. Tabary, “Inspection of Complex Geometries using radiographic simulation in CIVA”, 7th International Conference on NDE in Relation to Structural Integrity for Nuclear and Pressurized Components, 2009.
- [3] A.Schumm, O. Bremnes, B. Chassignole, «Numerical simulation of radiographic inspections: fast and realistic results even for thick components»Proceedings of the 16th world conference of Non-Destructive Testing, Montreal, aout 2004
- [4] J. Tabary, A. Glière, R. Guillemaud, P. Hugonnard, F. Mathy, « Combination of high resolution analytically computed uncollided flux images with low resolution Monte Carlo computed scattered flux images”, IEEE Transactions on Nuclear Science, Vol. 51, No. 1, pp 212-217, Feb 2004.
- [5] L.A. Feldkamp, I.C. Davis, J.W. Kress. Practical cone-beam algorithm. J. Opt. Soc. Am. A, 1(6):612–619, 1984.
- [6] H. Wang, X-ray CT Image Reconstruction from Few Projections, PhD Thesis, Joseph-Fourier University of Grenoble, 2011.
- [7] C. Li, W. Yin, and Y. Zhang. TV minimization by augmented Lagrangian and Alternating Direction Algorithms, 2009.